IEEE Photonics Journal
An IEEE Photonics Society Publication

Open Access

Silicon Based GeSn p-i-n Photodetector for SWIR Detection

Volume 8, Number 5, October 2016

Hui Cong
Chunlai Xue
Jun Zheng
Fan Yang
Kai Yu
Zhi Liu
Xu Zhang
Buwen Cheng
Qiming Wang

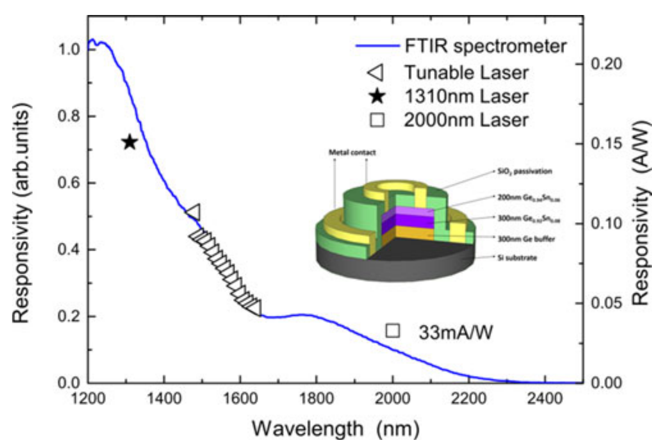

DOI: 10.1109/JPHOT.2016.2607687
1943-0655 © 2016 IEEE

IEEE photonics SOCIETY

IEEE

Silicon Based GeSn p-i-n Photodetector for SWIR Detection

Hui Cong, Chunlai Xue, Jun Zheng, Fan Yang, Kai Yu, Zhi Liu, Xu Zhang, Buwen Cheng, and Qiming Wang

State Key Laboratory on Integrated Optoelectronics, Institute of Semiconductors, Chinese Academy of Science, Beijing 100083, China

DOI:10.1109/JPHOT.2016.2607687
1943-0655 © 2016 IEEE. Translations and content mining are permitted for academic research only. Personal use is also permitted, but republication/redistribution requires IEEE permission. See http://www.ieee.org/publications_standards/publications/rights/index.html for more information.

Manuscript received June 21, 2016; revised September 6, 2016; accepted September 6, 2016. Date of publication September 8, 2016; date of current version September 28, 2016. This work was supported in part by the Major State Basic Research Development Program of China under Grant 2013CB632103; in part by the National Natural Science Foundation under Grant 61377045, Grant 61435013, Grant 61534005, and Grand 61604146; and in part by Beijing Natural Science Foundation under Grant 4162063. Corresponding author: C. Xue (e-mail: clxue@semi.ac.cn).

Abstract: We reported an investigation of GeSn-based p-i-n photodetectors (PDs) with a $Ge_{0.92}Sn_{0.08}$ active layer grown on n-type Si (100) substrate using molecular beam epitaxy (MBE). The GeSn photodetector achieved a wide spectrum detection whose cutoff wavelength can reach to 2.3 μm. The PDs exhibited a high performance near 2.0 μm with a responsivity of 93 mA/W and a dark current of 171 μA under a reverse bias of 1 V at room temperature. This work represented a promising technology to develop Si-based short-wave infrared (SWIR) photodetectors.

Index Terms: GeSn, photodetector, short-wave infrared (SWIR) imaging.

1. Introduction

Imaging in the short-wave infrared (SWIR) has attracted increasingly more attention in recent years. The SWIR wavelength from 1.4 μm to 3 μm responds primarily to the reflected light from objects, making objects easily recognized under weak visible light [1]. Imaging in the SWIR offers potential benefits such as imaging reflected star light at wavelength of 1.7 μm [2] and detection for CO_2 in both soil and air at wavelength of 2 μm [3]–[5]. In addition, hyperspectral remote sensing in SWIR has wide applications, such as mineralogy [6], environment [7], agriculture [8] and so on. The most appropriate materials for SWIR photodetectors are InGaAs and HgCdTe. However, the difficulties for focal-plane arrays (FPAs) fabrication limit these technologies' development and wide application. For example, InGaAs based photodetectors have to be bonded to silicon readout integrated circuits (ROICs) [9], and the mismatch of thermal expansion coefficients between the III-V PD and Si ROIC results in a low thermal cycle reliability [10]. Fortunately, $Ge_{1-x}Sn_x$ alloy with tunable direct bandgap from 0.8 eV to 0 eV has great potential in developing Si-based SWIR photodetectors, and this all group IV compound is totally compatible with the existing Si complementary metal–oxide semiconductor (CMOS) fabrication process. High-quality $Ge_{1-x}Sn_x$ film has been grown using chemical vapor deposition reactors (CVD) [11], molecular beam epitaxy (MBE) [12], and magnetron sputtering epitaxy [13], and PDs have also been fabricated through CMOS-compatible technology. As reported by many research groups, there are two kinds of GeSn photodetectors: p-i-n structure and photoconduction (PC) structure. An overview of the reported results is given in

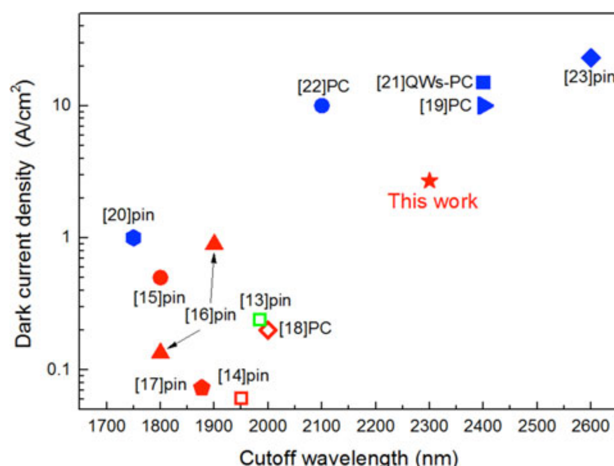

Fig. 1. Characteristics of GeSn photodetectors taken from different groups. The icons in blue, red, and green represent the GeSn alloy grown by CVD, MBE, and magnetron sputtering epitaxy, respectively. The solid icons indicate the devices fabricated on Si substrate, while the hollow ones correspond to Ge substrate. (The dark current densities of [19] and [21] are estimated values referred to [22].)

Fig. 1. Pham *et al.* [19] and Gassenq's group [21] reported photoconductive photodetectors with a cutoff wavelength of 2400 nm, and the GeSn layer was epitaxied on Si substrate by CVD reactor. However, the PC photodetectors are unlikely to achieve a low level of dark current and a high performance of radio frequency (RF) response. These disadvantages limit the development of PC photodetectors in the field of weak light detection and high speed imaging.

In this paper, we reported the fabrication and characterization of p-i-n photodetectors with a high quality $Ge_{0.92}Sn_{0.08}$ intrinsic layer and a p-type $Ge_{0.94}Sn_{0.06}$ layer grown on n-type Si substrate by the MBE process. The GeSn films were deposited on tensile strain Ge buffer in order to relieve compressive strain introduced by lattice mismatch. The results show that the GeSn p-i-n PDs have a wide spectral response covering most of the SWIR wavelength, and a high responsivity at 2.0 μm is achieved. Compared with other reported results, this work is likely to achieve a better sensitivity by improving the optical response and decreasing the dark current density, as shown in Fig. 1.

2. Material Growth and Device Fabrication

The samples were grown on a 4-inch n-type Si (100) wafer ($\rho = 0.002\,\Omega$ cm) using solid source molecular beam epitaxy. The structure consists of a) a 100 nm-thick low temperature (LT) and a 200 nm-thick high temperature (HT) Ge buffer, followed by cycle annealing between 900 °C and 600 °C five times [24]; b) a 300 nm-thick $Ge_{0.92}Sn_{0.08}$ layer grown at 180 °C; and c) a 200 nm-thick $Ge_{0.96}Sn_{0.06}$ cap layer grown at 180 °C. Before device fabrication, the boron (B) ions were implanted on the top of $Ge_{0.94}Sn_{0.06}$ layer with energy of 20 KeV and dose of $1.5 \times 10^{15}\,cm^{-2}$ and were annealed at 300 °C for 30 seconds in an N_2 atmosphere to form p^+-type $Ge_{0.94}Sn_{0.06}$. Devices were then fabricated using photolithography and Cl_2/BCl_3/Ar-based inductively coupled plasma (ICP) etching. The surface was covered by 650 nm-thick SiO_2 deposited using plasma-enhanced chemical vapor deposition (PECVD). Thirty nm-thick Ni and 800 nm-thick Al were deposited by electron beam evaporation to form metal contact for both GeSn alloy and Si substrate. The schematic cross section of GeSn p-i-n PD is shown in Fig. 2.

The strain of the layers and the Sn content in the $Ge_{1-x}Sn_x$ film layers are determined by high-resolution X-ray diffraction (HR-XRD) measurements in both (004) and (224) $\omega - 2\theta$ scanning. As shown in Fig. 3(a), the minimum full width at half maximum (FWHM) around (004) of intrinsic $Ge_{0.92}Sn_{0.08}$ layer and Ge buffer are 0.09° and 0.11°, respectively. In addition, the structural scanning transmission electron microscopy (STEM) image of the epitaxial layers is also shown in Fig. 3(b).

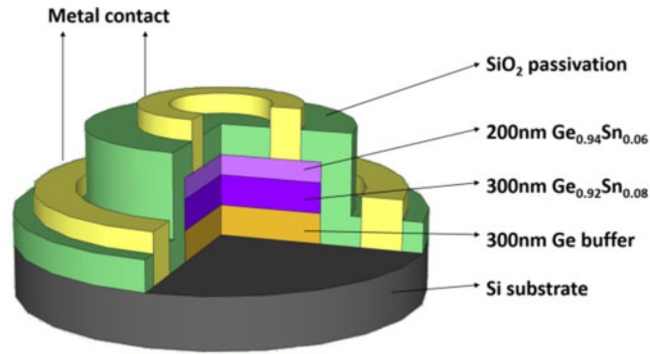

Fig. 2. Schematic cross of a top-illuminated GeSn p-i-n PD structure.

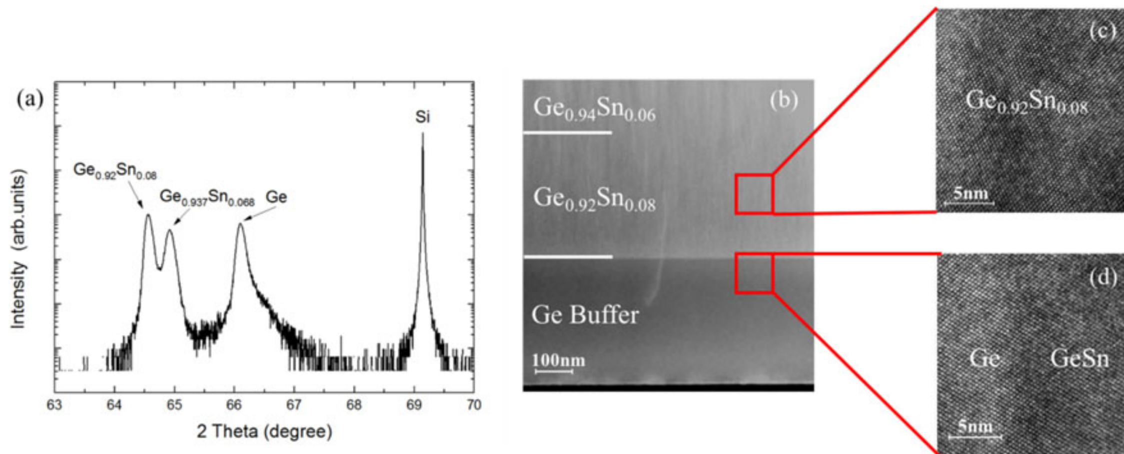

Fig. 3. (a) HR-XRD (004) ω-2θ scanning of GeSn alloy on Ge buffered Si substrate. (b) STEM image of $Ge_{0.94}Sn_{0.06}/Ge_{0.92}Sn_{0.08}$ alloy on Ge buffered Si (100). (c) HR-TEM image of $Ge_{0.92}Sn_{0.08}$ layer. (d) HR-TEM image of interface between $Ge_{0.92}Sn_{0.08}$ layer and Ge buffer layer.

TABLE 1
Summary of Lattice Constant, In-Plane Strain, and Sn Content

layer	$a_\perp$ (Å)	$a_\parallel$ (Å)	$\varepsilon_\parallel$	Sn content
Ge buffer	5.6504	5.6682	0.1973%	-
i-GeSn	5.7702	5.6753	−0.951%	8.1%
Top-GeSn	5.7419	5.6758	−0.6637%	6.3%

The crystal constant of bulk $Ge_{1-x}Sn_x$ material (a_{GeSn}) can be calculated using modified version of Vegard's law: $a_{GeSn} = a_{Ge}(1-x) + a_{Sn}x + bx(1-x)$, where b is the bowing parameter, which is 0.041 Å [25], and $a_{Ge} = 5.6587$ Å and $a_{Sn} = 6.4982$ Å are the bulk lattice constants for germanium and α-tin, respectively. The in-plane ($a_{||}$) and out-of-plane ($a_\perp$) lattice constants can be calculated from HR-XRD scanning. Then, the relaxed lattice constant of GeSn is determined by $a_{GeSn} = (a_\perp + 2a_{||}/\mu)/(1+2\mu)$, where $\mu = C_{12}/C_{11}$ is the ratio of two elastic constants which can be obtained by a liner interpolation between the ratio of Ge and Sn. The results are shown in Table 1. The Ge buffer contains a biaxial tensile strain of 0.1973% due to the different thermal expansion

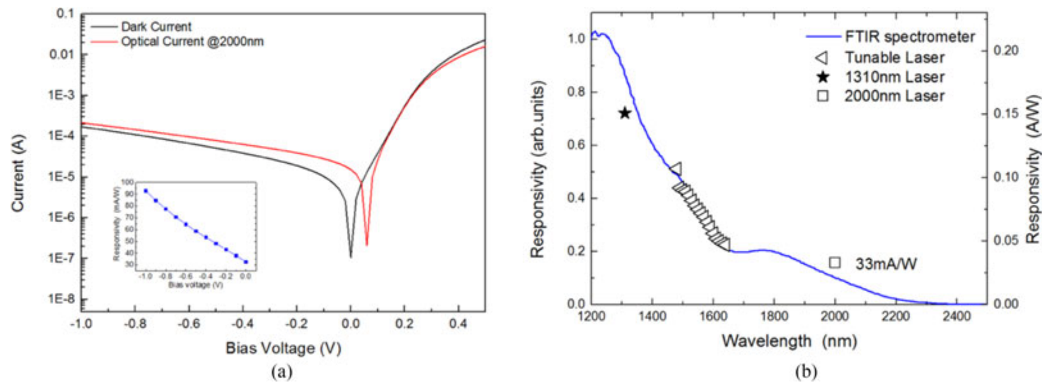

Fig. 4. (a) Dark current and photocurrent under the light of 2.0 μm of GeSn p-i-n PD with 90 μm-diameter mesa. (Inset) Optical responsivity of PD versus bias voltage at wavelength of 2.0 μm. (b) Optical responsivity of GeSn PD at 0 V, measured by a 1310 nm laser, a tunable laser (1480nm-1640nm), and a 2.0 μm laser. Spectrum response is measured using a FTIR spectrometer at zero operating voltage.

coefficient between Si and Ge [26]. This tensile strain can partially relieve compressive strain in upper GeSn layer, which extents the PDs cutoff wavelength. The degree of strain relaxation (R) of $Ge_{0.92}Sn_{0.08}$ layer is about 12%, indicating that the $Ge_{0.92}Sn_{0.08}$ active layer is highly strained. This is result from the high quality interface between Ge buffer and $Ge_{0.92}Sn_{0.08}$ layer, which is consistent with the high-resolution TEM image shown in Fig. 3(d).

3. Result and Discussions

The dark current and photocurrent of the GeSn photodetectors are measured by an Agilent B1500A Semiconductor Device Analyzer at room temperature. The optical response of the PD with a 90 μm-diameter mesa is obtained using a 1310 nm laser, a tunable laser (1440 nm–1640 nm), and a 2000 nm laser. The light to top of the device propagates through a single-mode lensed fiber. Spectral response of GeSn PD under a zero operating voltage is measured by a Nicolet 6700 Fourier transform infrared spectrometer (FTIR) with a KBr beam splitter and glow-bar source. A commercial InGaAs PD is tested for calibrating the spectrum responsivity.

As shown in Fig. 4(a), the dark current for device with 90 μm-diameter mesa is 171 μA at a reverse bias of 1 V, which is comparable with other reported values [20], [27], [28]. Generally speaking, the dark current rises up with increasing Sn content. It is due to (a) the misfit dislocations at the GeSn/Ge and Ge/Si interface; (b) threading dislocations in epitaxy GeSn alloy introduced from Ge buffer; and (c) raising of the intrinsic carriers owing to direct bandgap narrowing. The fabrication process can also bring about large surface leakage current, which can be reduced by Si passivation, as reported by Dong [17]. The inset shows the responsivity versus the applied voltage at a wavelength of 2000 nm. A high value of 93 mA/W is achieved under a reverse bias of 1 V, which is the maximum for a Si-based GeSn p-i-n photodetector as so far.

The spectral response of the GeSn PD is measured using FTIR spectrometer under zero bias at room temperature. As shown in Fig. 4(b), the trend of spectral response agrees well with that measured by tunable laser and special lasers. The response of GeSn PD continuously declines until wavelength of 1640 nm, which is corresponding to direct bandgap of tensile strain Ge (0.767 eV). The simulation of the energy band structure will be discussed later. As the wavelength increases further, the PD's response remains the same, which is attributed to the absorption of Ge indirect band gap and GeSn layers. Then, the optical response continuously decreases, and eventually, the spectral response achieves a cutoff wavelength at 2.3 μm.

To analyze the PD's spectral response, we consider that the energy bandgap of $Ge_{1-x}Sn_x$ alloy is adjusted by both biaxial strain and Sn content which was put forward by Van de Walle [29]. Average energy of germanium valence band is set as zero-point energy, and that of α-tin is 0.69 eV [30].

TABLE 2
Constants Used For Calculation of GeSn/Ge Energy Bandgap [29]–[32] (eV)

Material	$E_{v,av}$	a_v	a_c^{Γ}	a_c^{L}	Δ_0	b	E_g^{Γ}	E_g^{L}	b_{GeSn}^{Γ}	b_{GeSn}^{L}
Ge	0	1.24	−8.24	−1.54	0.3	−2.9	0.79	0.76	2.87	0.89
Sn	0.69	1.55	−6	−2.14	0.8	−2.7	−0.413	0.092		

The film volume variation under strain depends on $\Delta V/V = 2\varepsilon_{\|} + \varepsilon_{\perp} = 2(1 - C_{12}/C_{11})(a_{\|}/a - 1)$, where $\varepsilon_{\|}$ and $\varepsilon_{\perp}$ are the in-plane strain and out-of-plane strain, respectively. Then the change of average energy can be obtained by $\Delta E_{v,av} = a_v(\Delta V/V)$, where a_v is the hydrostatic potential for the valence band. The strain of Ge and GeSn layer can relieves the valence band spin degeneracy, then the energy of both heavy-hole and light-hole band can be calculated by the following equations:

$$E_{vL} = E_{v,av} + \Delta E_{v,av} - \Delta_0/6 + \delta E_{100}/4 + 1/2[\Delta_0^2 + \Delta_0 \cdot \delta E_{100} + 9/4\delta E_{100}^2]^{1/2} \quad (1)$$

$$E_{vH} = E_{v,av} + \Delta E_{v,av} + \Delta_0/3 - \delta E_{100}/2 \quad (2)$$

where Δ_0 is the energy of spin-orbit splitting band. In these equations, δE_{100} equals $2b(a_{\perp} - a_{\|})/a$, and b is the shear deformation potential for a strain of tetragonal symmetry. The bottom energy of conduction band (E_c) can be obtained from the sum of E_v, E_g, and ΔE_c. The energy of bandgap (E_g) is determined by $E_g = E_{g,Ge}(1 - x) + E_{g,Sn}x + b_{GeSn}x(1 - x)$, where b_{GeSn} is the energy bowing parameter. The above equations can also be applied to both Γ-valley and L-valley of conduction band. The parameters of GeSn alloy are obtained by linear interpolation, and Table 2 shows these parameters of bulk Ge and α-Sn, respectively. Thus, for the active $Ge_{0.92}Sn_{0.08}$ layer under 0.95% compress strain, the calculated direct bandgap between Γ-valley of conduction band and heavy-hole band is 0.543 eV, which agrees well with the measured spectral response edge around 2.3 μm (0.539 eV).

4. Conclusion

In summary, we have designed and fabricated a Si-based GeSn p-i-n photodetectors. A high-quality $Ge_{0.94}Sn_{0.06}/Ge_{0.92}Sn_{0.08}$ film was epitaxied on n-type Si (100) substrate MBE. The GeSn PD was fabricated by implementing a CMOS-compatible technology. The photodetector with a 90 μm-diameter mesa exhibited a high responsivity of 93 mA/W and a dark current of 171 μA at a reverse voltage of 1 V for the wavelength of 2.0 μm at room temperature. The spectral response measured by FTIR spectrometer showed a wide photodetection spectrum with a cutoff wavelength at 2.3 μm, covering most of the range of SWIR. The results indicate that the $Ge_{0.92}Sn_{0.08}$ PIN detector has a bright future, and it will be a prospective application in the SWIR field.

References

[1] M. P. Hansen and D. S. Malchow, “Overview of SWIR detectors, cameras, and applications,” *Proc. SPIE*, vol. 6939, 2008, Art. no. 69390I.
[2] M. H. Ettenberg, M. A. Blessinger, M. T. O’Grady, S.-C. Huang, R. M. Brubaker, and M. J. Cohen, “High-resolution SWIR arrays for imaging at night,” *Proc. SPIE*, vol. 5406, pp. 46–55, 2004.
[3] A. Joshi and S. Datta, “High-speed, large-area, pin InGaAs photodiode linear array at 2-micron wavelength,” *Proc. SPIE*, vol. 8353, 2012, Art. no. 83533D.
[4] A. Krier, H. Gao, and Y. Mao, “A room temperature photovoltaic detector for the mid-infrared (1.8-3.4 μm) wavelength region,” *Semicond. Sci. Technol.*, vol. 13, no. 8, pp. 950–956, 1998.

[5] N. Ye *et al.*, “AlInGaAs surface normal photodiode for 2 μm optical communication systems,” in *Proc. IEEE Photon. Conf.*, 2015, pp. 456–459.
[6] T. Cudahy *et al.*, “Mapping porphyry-skarn alteration at Yerington, Nevada, using airborne hyperspectral VNIR-SWIR-TIR imaging data,” in *Proc. IEEE Conf. Geosci. Remote Sens. Symp.*, 2001, pp. 631–633.
[7] D. F. Gleeson *et al.*, “Characterization of a sulfur-rich Arctic spring site and field analog to Europa using hyperspectral data,” *Remote Sens. Environ.*, vol. 114, no. 6, pp. 1297–1311, 2010.
[8] J. Xing, P. Van Hung, S. Symons, M. Shahin, and D. Hatcher, “Using a short wavelength infrared (SWIR) hyperspectral imaging system to predict alpha amylase activity in individual Canadian western wheat kernels,” *Sens. Instrum. for Food Quality Safety*, vol. 3, no. 4, pp. 211–218, 2009.
[9] T. Martin, R. Brubaker, P. Dixon, M.-A. Gagliardi, and T. Sudol, “640 $\times$ 512 InGaAs focal plane array camera for visible and SWIR imaging,” *Proc. SPIE*, vol. 5783, pp. 12–20, 2005.
[10] V. Bazovkin *et al.*, “High operating temperature SWIR p^+–n FPA based on MBE-grown HgCdTe/Si (013),” *Infrared Phys. Techn.*, vol. 76, pp. 72–74, 2016.
[11] H.-J. Jo, M. G. So, J. S. Kim, M.-Y. Ryu, Y. K. Yeo, and J. Kouvetakis, “Temperature-dependent direct transition energy in $Ge_{0.99}Sn_{0.01}$ film grown on Si measured by photoreflectance spectroscopy,” *Thin Solid Films*, vol. 591, pp. 295–300, 2015.
[12] M. Oehme *et al.*, “Epitaxial growth of highly compressively strained GeSn alloys up to 12.5% Sn,” *J. Cryst. Growth*, vol. 384, pp. 71–76, 2013.
[13] J. Zheng *et al.*, “GeSn pin photodetectors with GeSn layer grown by magnetron sputtering epitaxy,” *Appl. Phys. Lett.*, vol. 108, no. 3, 2016, Art. no. 033503.
[14] D. Zhang *et al.*, “High-responsivity GeSn short-wave infrared p-i-n photodetectors,” *Appl. Phys. Lett.*, vol. 102, no. 14, 2013, Art. no. 141111.
[15] H. H. Tseng *et al.*, “GeSn-based p-i-n photodiodes with strained active layer on a Si wafer,” *Appl. Phys. Lett.*, vol. 103, no. 23, 2013, Art. no. 231907.
[16] K. Ye *et al.*, “Absorption coefficients of GeSn extracted from PIN photodetector response,” *Solid-State Electron.*, vol. 110, no. 23, pp. 71–75, 2015.
[17] Y. Dong *et al.*, “Suppression of dark current in germanium-tin on silicon pin photodiode by a silicon surface passivation technique,” *Opt. Exp.*, vol. 23, no. 103, pp. 18611–18619, 2015.
[18] B. R. Conley *et al.*, “Infrared spectral response of a GeSn pin photodiode on Si,” in *Proc. IEEE Conf. Group IV Photon.*, 2014, pp. 17–18.
[19] T. Pham *et al.*, “Si-based $Ge_{0.9}Sn_{0.1}$ photodetector with peak responsivity of 2.85 A/W and longwave cutoff at 2.4 μm,” *Electron. Lett.*, vol. 51, no. 11, pp. 854–856, 2015.
[20] J. Mathews, R. Roucka, J. Xie, S.-Q. Yu, J. Menéndez, and J. Kouvetakis, “Extended performance GeSn/Si(100) p-i-n photodetectors for full spectral range telecommunication applications,” *Appl. Phys. Lett.*, vol. 95, no. 13, 2009, Art. no. 133506.
[21] A. Gassenq *et al.*, “GeSn/Ge heterostructure short-wave infrared photodetectors on silicon,” *Opt. Exp.*, vol. 20, no. 25, pp. 27297–27303, 2012.
[22] B. R. Conley *et al.*, “Temperature dependent spectral response and detectivity of GeSn photoconductors on silicon for short wave infrared detection,” *Opt. Exp.*, vol. 22, no. 13, pp. 15639–15652, 2014.
[23] T. Pham *et al.*, “Systematic study of Si-based GeSn photodiodes with 2.6 μm detector cutoff for short-wave infrared detection,” *Opt. Exp.*, vol. 24, no. 5, pp. 4519–4531, 2016.
[24] H.-C. Luan *et al.*, “High-quality Ge epilayers on Si with low threading-dislocation densities,” *Appl. Phys. Lett.*, vol. 75, no. 19, 1999, Art. no. 2909.
[25] F. Gencarelli *et al.*, “Crystalline Properties and Strain Relaxation Mechanism of CVD Grown GeSn,” *ECS J. Solid State Sci.*, vol. 2, no. 4, pp. P134–P137. 2013.
[26] J. Liu *et al.*, “Deformation potential constants of biaxially tensile stressed Ge epitaxial films on Si (100),” *Phys. Rev. B*, vol. 70, 2004, Art. no. 155309.
[27] J. Werner *et al.*, “Germanium-tin p-i-n photodetectors integrated on silicon grown by molecular beam epitaxy,” *Appl. Phys. Lett.*, vol. 98, no. 6, 2011, Art. no. 061108.
[28] M. Oehme *et al.*, “GeSn p-i-n detectors integrated on Si with up to 4% Sn,” *Appl. Phys. Lett.*, vol. 101, no. 14, 2012, Art. no. 141110.
[29] C. G. Van de Walle, “Band lineups and deformation potentials in the model-solid theory,” *Phys. Rev. B*, vol. 39, no. 3, pp. 1871–1883, 1989.
[30] H. Pérez Ladrón de Guevara, A. G. Rodríguez, H. Navarro-Contreras, and M. A. Vidal, “Nonlinear behavior of the energy gap in $Ge_{1-x}Sn_x$ alloys at 4K,” *Appl. Phys. Lett.*, vol. 91, no. 16, 2007, Art. no. 161909.
[31] W.-J. Yin, X.-G. Gong, and S.-H. Wei, “Origin of the unusually large band-gap bowing and the breakdown of the band-edge distribution rule in the Sn_xGe_{1-x} alloys,” *Phys. Rev. B*, vol. 78, no. 16, 2008, Art. no. 161203.
[32] N. Yahyaoui, N. Sfina, J. L. Lazzari, A. Bournel, and M. Said, “Band engineering and absorption spectra in compressively strained $Ge_{0.92}Sn_{0.08}$/Ge (001) double quantum well for infrared photodetection,” *Phys. Status Solidi C*, vol. 11, no. 11–12, pp. 1561–1565, 2014.